High-pressure phase diagram of the exp-6 model: The case of Xe

Franz Saija[1,*] and Santi Prestipino[2,†]
[1]*CNR, Istituto per i Processi Chimico-Fisici, sezione Messina, via La Farina 237, 98123 Messina, Italy*
[2]*Università degli Studi di Messina, Dipartimento di Fisica, Contrada Papardo, 98166 Messina, Italy*
(Received 6 October 2004; revised manuscript received 24 March 2005; published 20 July 2005)

We investigated numerically the high-temperature–high-pressure phase diagram of xenon as modeled through the exp-6 interaction potential, which is thought to provide a reliable description of the thermal behavior of rare gases under extreme conditions. We performed a series of extensive *NVT* Monte Carlo simulations which, in conjunction with exact computation of the solid free energy by the Frenkel-Ladd method, allowed us to precisely locate the freezing and melting thresholds at each temperature. We find that, under isothermal compression, the exp-6 fluid freezes directly into a fcc solid; however, above 4500 K, an intermediate bcc phase becomes stable in a narrow range of pressures. The chemical potential of the hcp phase never significantly differs from that of the fcc solid of equal T and P, though the former is found to be slightly greater than the latter. We discuss our results in the light of previous numerical studies of the same model system and of the experimental data available for xenon.

DOI: 10.1103/PhysRevB.72.024113 PACS number(s): 61.20.Ja, 05.20.Jj, 64.10.+h, 64.70.Kb

I. INTRODUCTION

In the last decade, there has been an increasing interest in the high-temperature–high-pressure (HT-HP) properties of many materials,[1–3] as realized for instance in the deep core of the planets of our solar system. Such peculiar conditions do in fact provide an additional means for testing current condensed-matter theories, since squeezing matter to planetary pressure and heating it up to a few thousand degrees can trigger various forms of structural reorganization both at the macroscopic and at the molecular level (see, for instance, the two paradigmatic cases of water and methane), or even cause modifications in the electronic transport properties (as happens for, e.g., hydrogen). Since down-the-earth experiments are somewhat limited (pressure can hardly be pushed over a certain threshold and, more important, any huge compression is plagued by severe nonhydrostaticity problems), the only possible insights into the transformations undergone by many substances at extreme conditions often come from numerical simulation—provided, however, a theoretical model of that substance is amenable to careful investigation and numerical errors are kept under control.

Due to their closed electronic shells, (heavy) rare gases are usually believed to be the simplest substances of all; hence it may appear somewhat strange that their thermal behavior in the HT-HP regime (i.e., in the very dense fluid and solid regions) is not yet well assessed.[4] Despite the fact that one can get rid of quantum-mechanical considerations almost completely (at a temperature as high as 3500 K, it was shown in Ref. 5 that electronic excitations do not play any significant role up to pressures of order 50 GPa), a classical interaction potential that accurately reproduces the thermodynamic properties of rare gases cannot be of the simple Lennard-Jones form. In fact, while performing very well at ambient conditions, the Lennard-Jones potential loses much of its reliability when temperature and pressure take huge values. For high system densities, three-body contributions to the effective potential are likely to be as important as the two-body term,[6] with the effect that the atomic core is softer than implied by the Lennard-Jones interaction. If one insists in using a two-body effective potential, a more reliable form for rare gases turns out to be the (modified) Buckingham or exp-6 potential[7] [see it defined in Eq. (2.1)], as parametrized through high-density experimental data.[8] As a matter of fact, when HT-HP conditions hold, an exponential law is a more adequate representation for the interatomic repulsion at short distances than is a power law. In this respect, we can say that the exp-6 potential takes into account the effects of the three-body interaction in an isotropic fashion.

Recently, some controversy has arisen about the topology of the HT-HP part of the phase diagram of Xe, whose behavior should be representative also of Ar and Kr. Stimulated by the findings of a recent laser-heated diamond-anvil-cell (DAC) experiment on Xe,[9] Belonoshko *et al.* have done molecular-dynamics (MD) computer simulations of the exp-6 potential in order to interpret those data.[5,10] In the DAC experiment, a Xe fluid sample is compressed at a given pressure in the range between 10 and 40 GPa and subsequently heated with a laser until a bulk transition is detected. The experiment is meant to provide information about the freezing of fluid Xe in the HT-HP region and, ultimately, to draw the fluid-solid coexistence line in the P-T diagram. Surprisingly, the freezing line shows an unexpected cusp near $T=2700$ K and $P=15$ GPa, which was originally imputed to the boundary between a fluid-solid and a fluid-glass transition.[9] The numerical simulations of the exp-6 model by Belonoshko *et al.* have instead revealed a competition between two distinct, fcc and bcc solid phases, which happen to exchange their relative thermodynamic stability right in the region of the observed cusp. More precisely, for temperatures above $T\simeq 2700$ K, a fluid-bcc-fcc sequence of phases is reported upon isothermically increasing the pressure beyond 25 GPa. This interpretation has been criticized by Kechin.[11]

The simulation method used in Refs. 5 and 10 was the so-called two-phase or coexistence method,[12,13] as implemented in an isothermal-isobaric MD simulation.[14] In point of principle, this technique should be able to detect a coex-

istence between two structurally distinct phases whenever it occurs; in practice, this method has some limitations since it requires large sizes and very long simulation times to reach good equilibration in the region of the interface between the coexisting phases.[15] Moreover, it cannot be excluded that the route to equilibrium of an unstable interface will pass through (and long remain in) a phase which, though not being the preferred one under bulk conditions, is nonetheless promoted by (small) spatial inhomogeneities of the system. This would be especially so when the difference in Gibbs free energy between two distinct solid phases is very small: in that case, a system being prepared in a metastable solid phase would take a very long time (possibly much longer than is accessible to simulation) to relax to the truly stable solid.

In order to gain further insight into the nature of Xe freezing at the temperatures investigated by the DAC experiment, we have carried out a Monte Carlo simulation in the canonical ensemble of the same exp-6 system of Refs. 5 and 10, but now calculating the free energy of the relevant solid phases by the method of Frenkel and Ladd,[16] which would provide the benchmark for solid-free-energy evaluations. When used in conjunction with conventional thermodynamic integration, this method would allow one to draw the "exact" phase diagram of the given model system and the only source of error would be associated with the finite size of the sample. Indeed, if the chemical-potential gaps between different solid structures are minute, also the statistical errors affecting the relevant thermodynamic averages are to be made sufficiently small (i.e., by carrying out long enough simulation runs). As a matter of fact, we neither confirm the findings of Belonoshko *et al.*—for we predict that the bcc solid would become stable in Xe only above 4500 K—nor find any good agreement with the DAC data of Ref. 9 at the highest temperatures, i.e., no clear bump is seen along the freezing line. A similar outcome was also found by Frenkel for He,[17] whose bcc-fcc transition would only occur in a region of the phase diagram where the fluid is stable.

The outline of the paper is the following. In Sec. II, we introduce the model system and describe our simulation method. In Sec. III, we present our numerical results and draw the ensuing phase diagram. Then, in Sec. IV, we make a critical comparison of our outcome with those of previous studies. Further comments and remarks are postponed to the Conclusions.

II. MODEL AND METHOD

A. The exp-6 model

All textbooks in statistical mechanics report that rare-gas thermal behavior is well accounted for by the simple Lennard-Jones pair potential. However, it is less known that, when rare gases are *very dense*, a different potential with a softer repulsive shoulder is better suited. Such is the exp-6 potential, defined to be

$$v(r)=\begin{cases}+\infty, & r<\sigma,\\ \dfrac{\epsilon}{\alpha-6}\left\{6\exp\left[\alpha\left(1-\dfrac{r}{r_m}\right)\right]-\alpha\left(\dfrac{r_m}{r}\right)^6\right\}, & r\geqslant\sigma,\end{cases} \tag{2.1}$$

where α controls the softness of the repulsion and $\epsilon>0$ is the depth of the potential minimum located at r_m. We select the value of σ in such a way that, for the given α and r_m, the function appearing in the second line of Eq. (2.1) reaches its maximum right at σ. Hence, as r moves down to σ, $v(r)$ reaches a stationary value and then goes abruptly to infinity. Ross and Mc Mahan have shown that, for a suitable choice of the parameters α, ϵ, and r_m, $v(r)$ gives a rather faithful representation of many thermodynamic properties of Ar at high densities. Moreover, a corresponding-state theory appears to hold, which permits us to derive the model parameters appropriate to Kr and Xe from those of Ar. For Xe, such best parameters are $\alpha=13$, $\epsilon/k_B=235$ K, and $r_m=4.47$ Å,[8] where k_B is the Boltzmann constant (for $\alpha=13$, the value of σ is then $0.246\,972\ldots r_m$). In the following, we work with dimensionless variables, i.e., $T^*=k_BT/\epsilon$, $P^*=Pr_m^3/\epsilon$, and $\rho^*=\rho r_m^3$ ($\rho\equiv N/V$ is the particle-number density). The accuracy of the exp-6 modelization for xenon at low pressures was tested by Belonoshko *et al.* against available experimental results and, up to 0.7 GPa, was found to be good (see Fig. 7 of Ref. 5).

Recently, the vapor-liquid equilibria of the exp-6 fluid were studied numerically through a series of Monte Carlo (MC) simulations in the Gibbs ensemble.[18] As a result, the critical point was located at $\rho^*=0.303$ and $T^*=1.316$. From a simulation study by Errington and Panagiotopoulos a slightly different estimate of the critical-point coordinates is extracted, namely, $\rho^*=0.318$ and $T^*=1.318$.[19] Finally, the freezing density of the exp-6 fluid was estimated for a number of temperatures by the Hansen-Verlet criterion.[20,21]

B. Details of the Monte Carlo simulation

The numerical-simulation method provides virtually exact information on the statistical behavior of a given model system. We have performed Monte Carlo simulations of the exp-6 model in the canonical ensemble (i.e., at constant temperature T, volume V, and number N of particles), using the standard Metropolis algorithm for sampling the equilibrium distribution in configurational space. The only values of N that we consider are those that fit a cubic simulation box with an integer number of cells, i.e., $N=4n^3$ for the fcc solid and $N=2n^3$ for the bcc solid, n being the number of cells along any spatial direction. For a given particle number, the length L of the box is adjusted to a chosen density value ρ, i.e., $L=(N/\rho)^{1/3}$. If a is the distance between two nearest-neighbor reference lattice sites, we have $a=(\sqrt{2}/2)(L/n)$ for a fcc crystal and $a=(\sqrt{3}/2)(L/n)$ for a bcc crystal. Finally, periodic conditions are applied to the box boundaries.

Our largest sample sizes were $N=1372$ (fcc) and $N=1458$ (bcc) which, to all practical purposes, can be regarded as nearly the same size. We point out that comparing the statistical properties of similar (large) sizes is mandatory

when we want to decide which solid phase is stable at given T and P, since this produces comparable statistical errors for the two phases. Otherwise, one can resort to some extrapolation to the thermodynamic limit which is, however, computationally far more demanding.

Some x-ray diffraction studies indicate that the fcc-hcp transition could be a common behavior in all rare-gas solids.[22–24] At room temperature, the hcp solid would be stable above 75 GPa, while metallization is not expected before $\approx$130 GPa.[25] We have thus carried out also a number of simulations of a hcp crystal hosting $10\times12\times12=1440$ particles [the simulation box is only approximately cubic in this case and the z axis is now oriented along the [111] direction—the three box sides have lengths of $L_x=n_x a$, $L_y=(\sqrt{3}/2)n_y a$, and $L_z=(\sqrt{6}/3)n_z a$, with $n_x=10$, $n_y=n_z=12$, and $a=(\sqrt{2}/\rho)^{1/3}$].

To locate the transition point at a given T, we have numerically generated two isothermal quasistatic paths, starting from the very dilute fluid on one side and from the highly compressed solid on the other side. As a rule, in the solid region, the last MC configuration produced at a given ρ serves, after suitable rescaling of particle coordinates, as the starting configuration for the run at a slightly lower density. Similarly, in the dense-fluid region, the simulations are carried out in a chain, i.e., the run at a given density is started from the last (rescaled) configuration produced at a lower ρ value. The fcc and bcc solid paths are followed until the fluid spontaneously forms during the MC run, as evidenced by the abrupt change in energy and pressure. Usually, we were able to overheat the solid for a little beyond the fluid-solid phase boundary, while undercooling of the fluid is much easier. For each ρ and T, equilibration of the sample typically takes 2×10^3 MC sweeps, a sweep consisting of one attempt to sequentially change the position of all particles. The maximum random displacement of a particle in a trial MC move is adjusted once a sweep during the run so as to keep the acceptance ratio of the moves as close to 50% as possible, with only small excursions around this value.

For given NVT conditions, the relevant thermodynamic averages are computed over a trajectory whose length ranges from 2×10^4 to 6×10^4 sweeps. The excess energy per particle $u_{\rm ex}$, the pressure P, and (in the solid phase) the mean square deviation δR^2 of a particle from its reference lattice position are especially monitored. Pressure comes from the virial formula

$$P=\rho k_B T+\frac{\langle\mathcal{V}\rangle}{V},\quad \mathcal{V}=-\frac{1}{3}\sum_{i<j} r_{ij}v'(r_{ij}) \tag{2.2}$$

(r_{ij} is the distance between particles i and j). In practice, to avoid double counting of interactions, the pair potential is truncated above a certain cutoff distance r_c, which is taken to be only slightly smaller than $L/2$. Then, the appropriate long-range corrections are applied to energy and pressure by assuming $g(r)=1$ beyond r_c, $g(r)$ being the radial distribution function (RDF).

The RDF histogram is constructed with a spatial resolution of $\Delta r=r_m/50$ and updated every ten MC sweeps. The RDF is computed up to a distance of $L/2$: at that distance, the $g(r)$ was never found to significantly differ from unity, at least for the largest system sizes.

To evaluate the numerical errors affecting the main statistical averages, we divide the MC trajectory into ten blocks and estimate the length of the error bars as being twice the empirical standard deviation of the block averages from the mean (under the implicit assumption that the decorrelation time of any relevant variable is less than the size of a block). Typically, the relative errors of energy and pressure are a few tenths of a percent.

The difference in excess free energy between two equilibrium states of the system, say 1 and 2, lying *within the same phase* is computed through the combined use of the formulas

$$\frac{f_{\rm ex}(T_2,\rho)}{T_2}=\frac{f_{\rm ex}(T_1,\rho)}{T_1}-\int_{T_1}^{T_2}dT\frac{u_{\rm ex}(T,\rho)}{T^2} \tag{2.3}$$

and

$$\beta f_{\rm ex}(T,\rho_2)=\beta f_{\rm ex}(T,\rho_1)+\int_{\rho_1}^{\rho_2}d\rho\frac{1}{\rho}\left[\frac{\beta P(T,\rho)}{\rho}-1\right], \tag{2.4}$$

where $f_{\rm ex}$ is the excess Helmholtz free energy per particle and $\beta=(k_B T)^{-1}$. The integrals in Eqs. (2.3) and (2.4) are performed numerically by applying the Simpson rule to a linear-spline approximant of the simulation data for energy and pressure.

The above formulas are, however, useless if one does not have an independent estimate of the system free energy in a reference state. Only in this case do Eqs. (2.3) and (2.4) help in finding the free energy of any other state in the same phase. The choice of such a reference state is different for the fluid and solid phases. As a reference state for the fluid, we can choose any equilibrium state that is characterized by a very small ρ value and arbitrary T (say, a nearly ideal gas), since then the excess chemical potential of the system can be accurately estimated by the Widom or particle-insertion method,

$$\mu_{\rm ex}=-k_B T\ln\langle\exp(-\beta E_{\rm ins})\rangle, \tag{2.5}$$

where $E_{\rm ins}$ comprises all interaction terms between a randomly inserted ghost particle and all the system particles. The average in Eq. (2.5) is evaluated numerically during a run of typically 5×10^4 equilibrium sweeps, with an insertion attempted at the completion of every sweep. Once $\mu_{\rm ex}$ is given, the excess values of free energy and entropy will follow from

$$\beta f_{\rm ex}=\beta\mu_{\rm ex}-\frac{\beta P}{\rho}+1 \text{ and } \frac{s_{\rm ex}}{k_B}=\beta(u_{\rm ex}-f_{\rm ex}). \tag{2.6}$$

It is useful to note that, from a strictly numerical point of view, choosing a very dilute gas as a reference state for the fluid is far better than starting the thermodynamic integration in Eq. (2.4) from the ideal gas of equal temperature. In fact, unless one has a lot of thermodynamic points in the very dilute region of the phase diagram, a spline interpolant of $\beta P/\rho$ that is sufficiently accurate in this region is hard to construct.

C. The Frenkel-Ladd calculation of solid free energies

The Frenkel-Ladd (FL) method for calculating the free energy of a solid system relies on a different kind of thermodynamic integration.[16,26] The idea is to continuously transform the system of interest with potential energy V_1 into a reference solid system of known free energy (typically, an Einstein crystal). This is accomplished through a linear interpolation of the potential-energy functions V_0 and V_1 of the two systems, i.e., $V_\lambda = V_0 + \lambda(V_1 - V_0)$ (with $0 \leqslant \lambda \leqslant 1$). Then, the difference in free energy between two homologous *NVT* states of the systems is calculated via the exact Kirkwood formula

$$F_1 - F_0 = \int_0^1 d\lambda \langle V_1 - V_0 \rangle_\lambda, \tag{2.7}$$

where the average $\langle \cdots \rangle_\lambda$ is taken over the equilibrium distribution of the hybrid system with V_λ potential and is evaluated numerically by a Monte Carlo procedure.

Upon denoting by $\{\mathbf{R}_i^{(0)}, i=1,\ldots,N\}$ the reference lattice positions, the Einstein model is described by an interaction potential of

$$V_{\mathrm{Ein}}(\mathbf{R}^N) = \frac{1}{2} c \sum_{i=1}^{N} (\mathbf{R}_i - \mathbf{R}_i^{(0)})^2, \tag{2.8}$$

where c is the spring constant—the same for all oscillators. It readily follows from Eq. (2.8) that the free energy and mean square separation of a particle from its reference lattice site are given by

$$\beta F_{\mathrm{Ein}} = -\frac{3N}{2} \ln\left(\frac{2\pi}{\beta c \Lambda^2}\right) \text{ and } \delta R^2_{\mathrm{Ein}} = \frac{3}{\beta c}, \tag{2.9}$$

where Λ is the thermal wavelength. In deriving the first of Eqs. (2.9), no Gibbs factor of $N!$ was included in the partition function since the Einstein oscillators are distinguishable entities.

A nontrivial problem with this choice of reference system, already pointed out in the original article,[16] is the following: while the Einstein particles can only perform limited excursions around their reference positions, which implies a finite value of δR^2, there is no means to constrain particles interacting through V_1 to remain confined in the neighborhood of their initial positions, even in the solid phase. In other words, at variance with V_{Ein}, V_1 is a translationally invariant potential, with the result that the integrand in Eq. (2.7) shows a divergence, in the thermodynamic limit, at $\lambda = 1$. To overcome this problem, Monte Carlo simulations of V_λ are usually performed under the constraint of a fixed center of mass. We do not repeat here the entire analysis showing how to deal with such a constraint in the equilibrium sampling, but simply quote the final result (see Ref. 26 for details):

$$\beta f_{\mathrm{ex}} \equiv \beta \frac{F - F_{\mathrm{id}}}{N} = -\ln[\rho(\beta c)^{-3/2}] - \frac{3}{2}\ln(2\pi) + 1 - \frac{2\ln N}{N} + \frac{\ln(2\pi)}{N} + \frac{\ln[\rho(\beta c)^{-3/2}]}{N} + \frac{\beta}{N}\int_0^1 d\lambda \langle \Delta V \rangle_\lambda^{\mathrm{c.m.}}, \tag{2.10}$$

where the superscript c.m. denotes a constrained average and $\Delta V = V_1 - V_0$. Polson *et al.* have conjectured that, on fairly general grounds, $\beta f_{\mathrm{ex}}(N) + \ln N/N = \beta f_{\mathrm{ex}}(\infty) + O(N^{-1})$.[26] We shall see later whether this is found in our case. Given the value of f_{ex}, the excess chemical potential of the solid still follows from the first of Eqs. (2.6).

A few considerations on the numerical implementation of the FL method are now in order. While in principle the value of c can be chosen arbitrarily, just for numerical purposes it is convenient to take it such that δR^2 of the target solid is close to $3/(\beta c)$: in this case, the variations of the integrand in Eq. (2.7) with λ are likely to be small as well as the error in performing the numerical quadrature.

A further caveat must be added for hard-core potentials (as is the one we are interested in here). If we write the potential as the sum of a hard-sphere part plus a remainder, $V_1 = V_{\mathrm{HS}} + V_r$, then it is mandatory to include a V_{HS} term also in V_0, since otherwise there is no way to transform continuously from V_1 to V_0. As a result,

$$V_\lambda = V_{\mathrm{HS}} + V_{\mathrm{Ein}} + \lambda(V_r - V_{\mathrm{Ein}}), \tag{2.11}$$

implying $\Delta V = V_r - V_{\mathrm{Ein}}$ in Eq. (2.10). However, the free energy of a system of hard-core (that is, mutually interacting) Einstein particles is not known; what we can say is only that this interaction cannot have any consequence on the thermodynamic quantities of an Einstein crystal in so far as c takes sufficiently large values, since in this case particles are blind to each other. Then, unless c is given a huge value, the FL calculation is only viable for a very cold solid.

Whether a value of c is huge or not can be decided from the comparison between $\sqrt{3/(\beta c)}$ and $(a-\sigma)/2$. Should the former be much smaller than the latter, the error committed in assuming the form (2.9) for the free energy of the interacting Einstein crystal is presumably negligible. Frenkel and Ladd have indicated a more rigorous method to ascertain the importance of hard-core interactions for the free energy of an Einstein solid, based on the estimate of the leading (virial) correction to the free energy of the noninteracting Einstein particles.[16]

III. RESULTS

A. Test calculations

We first checked our FL simulation code against the hard-sphere calculation given in Ref. 26. We take a system of $N = 256$ hard spheres of diameter σ at $\rho\sigma^3 = 1.0409$ (this is about the melting density of the fcc solid), with $c = 6000 k_B T/\sigma^2$. We estimate numerically the average of $\Delta V = -V_{\mathrm{Ein}}$ over the canonical distribution relative to V_λ for a number of λ values in the range from 0 to 1. Precisely, we take λ to increase in steps of 0.05 from 0 to 0.9, with a

TABLE I. Excess free energy per particle in units of k_BT for a number of exp-6 solid states. For each state and solid type, also shown within square brackets is the value of $c^*=cr_m^2/\epsilon$ that is used in the Frenkel-Ladd calculation: for the chosen c^*, $\delta R^2_{\mathrm{Ein}}$ approximately matches the average square deviation of an exp-6 particle from its position in the perfect crystal.

βf_{ex}	fcc ($N=1372$)	hcp ($N=1440$)	bcc ($N=1458$)
$\rho^*=4$, $T^*=4.25$	38.879(1) [8500]		39.446(2) [5100]
$\rho^*=3.5$, $T^*=8.15$	16.258(1) [5400]		16.408(2) [3000]
$\rho^*=4$, $T^*=12.77$	17.216(1) [7700]		17.316(2) [5300]
$\rho^*=5$, $T^*=16$	25.654(1) [15000]	25.659(1) [14500]	25.784(2) [9100]
$\rho^*=5.5$, $T^*=20$	27.289(1) [19600]	27.295(1) [19400]	27.397(2) [13600]
$\rho^*=5$, $T^*=25$	18.489(1) [13800]	18.494(1) [14300]	18.532(2) [10100]

smaller step of 0.01 in the range from 0.9 to 1. For each value of λ, as many as 2×10^4 MC sweeps are produced at equilibrium. The MC moves are such that the position of the system center of mass is fixed; for the same purpose, if a particle happens to move (slightly) out of the simulation box, no attempt is made to put it back into the box.[27] In addition to the value of $\langle\Delta V\rangle_\lambda$, we also estimate the statistical error affecting this quantity by partitioning the MC trajectory into large blocks. Finally, the integral over λ in Eq. (2.10) is calculated using the Simpson rule. For the chosen c value, the virial correction to the free energy of the Einstein crystal due to hard-core interaction between particles is negligible ($\beta\Delta f_{\mathrm{ex}}\approx10^{-8}$). We thus find $\beta f_{\mathrm{ex}}+\ln N/N=5.891(5)$ for the fcc solid, which is fully consistent with the result obtained by Polson *et al.* (see Fig. 2 of Ref. 26).

As a further check of our numerical code, we have considered a model system of soft spheres interacting through the repulsive potential $v(r)=\epsilon(\sigma/r)^{12}$. We take a system of $N=256$ particles with $k_BT/\epsilon=1$, $\rho\sigma^3=1.1964$, and $c=500\,\epsilon/\sigma^2$. We estimate numerically the average of $\Delta V=V_1-(V_1^{(0)}+V_{\mathrm{Ein}})$ over the canonical distribution relative to V_λ for a number of λ values in the range from 0 to 1 ($V_1^{(0)}$ is the total potential energy as calculated for particles located in the respective perfect-lattice positions). For such ΔV, the quantity $\beta V_1^{(0)}/N$ must be added to the right-hand side of Eq. (2.10) to obtain βf_{ex}. For each value of λ, as many as 5×10^4 MC sweeps are produced at equilibrium. In the end, we find $\beta f_{\mathrm{ex}}+\ln N/N=9.208(2)$ for the fcc solid, which again perfectly agrees with Fig. 1 of Ref. 26.

B. The exp-6 simulation

Moving to the exp-6 model, we have calculated the excess free energy of both the fcc and the bcc solids for a number of (ρ^*,T^*) pairs, using for the integral in Eq. (2.10) the same specifications as given above for the test calculation on hard spheres. Though one single free-energy calculation by the FL method would be sufficient for estimating the free energy of the solid in any other state, we have often found it more practical to repeat the FL calculation rather than generating a long thermodynamic path to a very distant point in the phase diagram. In Table I, we collect the calculated values of the excess free energy per particle in a few state points, for three different solid phases of the exp-6 model (and for just the largest sizes). The numerical precision reported for each βf_{ex} is the Simpson integral of the errors that are associated with the values of $\beta\langle\Delta V\rangle_\lambda^{\mathrm{c.m.}}/N$, as calculated for the selected λ points.[28] In the same table, we indicate the value of $c^*=cr_m^2/\epsilon$ that is considered for each single state. In every case, this c is such that $3/(\beta c)\simeq\delta R^2$ of the exp-6 solid. Since all of the tabulated state points lie sufficiently far from the melting line, the average square excursion of an exp-6 particle from its reference lattice site turns out to be quite small. Hence, all of the c^*'s are much larger than 1 and the virial correction to the Einstein-crystal free energy is absolutely negligible.

We get an indirect check of the free-energy values in Table I by calculating, via ordinary thermodynamic integration based on Eqs. (2.3) and (2.4), the difference in excess free energy between various pairs of bcc and fcc states in the table. We have always found a perfect agreement with the tabulated values, to within the reported numerical precision, for both types of solids. For each (ρ^*,T^*) pair in Table I, we have finally verified that the linear scaling of $\beta f_{\mathrm{ex}}(N)+\ln N/N$ as a function of N^{-1} holds well, as demonstrated in Fig. 1 in one case only.

In order to see whether a stable bcc phase exists above $T^*\simeq11$ (which is where the authors of Ref. 5 would locate the fluid-bcc-fcc triple point), we have carried out extensive MC simulations of the exp-6 model for a number of T^* values (4.25, 8.15, 12.77, 16, 20, and 25). For all such values, we construct the fluid path and two solid, fcc and bcc paths (for $T^*=4.25$, only the fcc equation of state is generated). For $T^*=16$, 20, and 25, we have also constructed the equation of state for $N=1440$ particles in a hcp arrangement. With the only exception of $T^*=4.25$, where $N=864$, the other isotherms are plotted for $N=1372$ (fluid and fcc) and $N=1458$ (bcc) particles. Once the free energy of the system is known along an isothermal path, the chemical potential μ along the same path readily follows from the first of Eqs. (2.6) as a function either of ρ or, equivalently, of P. For given T and P values, the thermodynamically stable phase is the one with lower μ: hence, the phase transition from fluid to, e.g., fcc at constant temperature is located at the pressure where the chemical potential of the fluid takes over the μ of the fcc solid.

Surprisingly, we find that, at variance with the conclusions of Ref. 5 and 10, the bcc phase of the exp-6 model is

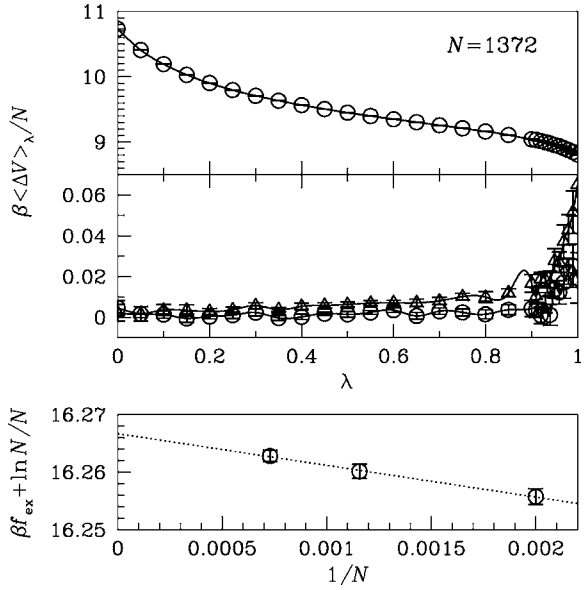

FIG. 1. Frenkel-Ladd calculation of solid free energies: fcc solid at $\rho^*=3.5$ and $T^*=8.15$. Top: the integrand of Eq. (2.10) is plotted in the panel above for $N=1372$ (the continuous line is a spline interpolant of the data points and the error bars, which are also shown, are much smaller than the symbol size). In the panel below, the finite-size effect is demonstrated for $\beta\langle\Delta V\rangle_\lambda/N$ through the difference between $N=500$ and 1372 (△) and between $N=864$ and 1372 (○). Bottom: the values of $\beta f_{ex}(N)+\ln N/N$ (for $N=500, 864$, and 1372) scale linearly with N^{-1} for large N, as conjectured in Ref. 26. We have verified that the same type of scaling holds for all of the solid-state points in Table I.

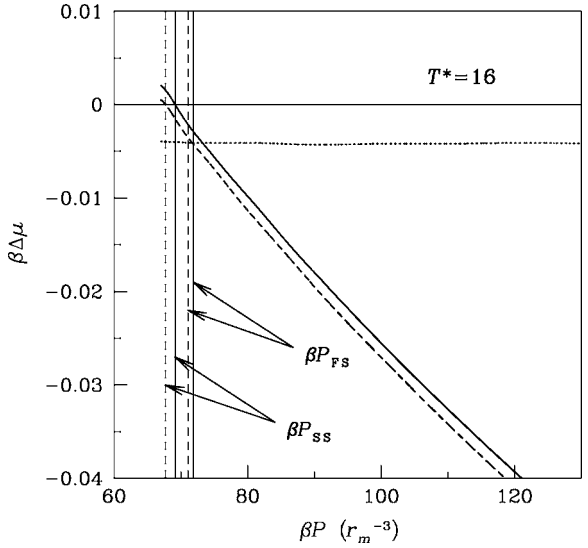

FIG. 2. Reduced chemical potential of the fcc solid relative to bcc and to hcp for $T^*=16$. Upon plotting the difference in $\beta\mu$ between fcc and bcc phases ($N=1372$ vs 1458, continuous line; $N=864$ vs 1024, dashed line), we find that, as pressure grows, the bcc phase loses stability to the advantage of fcc. All the plotted lines are linear-spline interpolants of the data points. The dotted line is the quantity $\beta(\mu_{fcc}-\mu_{hcp})$ ($N=1372$ for the fcc solid; $N=1440$ for the hcp solid). The two couples of vertical lines mark, from left to right, the position of the "virtual" transition between bcc and fcc and the fluid-fcc phase transition.

only stable at very high temperatures, i.e., above $T^*\simeq 20$, and in a narrow pressure interval. For all reduced temperatures up to 16, the scenario is similar (see it represented in Figs. 2 and 3 for $T^*=16$): as pressure grows, the chemical potential of the fluid eventually overcomes that of the fcc solid; at the crossing point P_{FS}, the latter is already lower than the bcc chemical potential. The bcc solid would be more stable than the fcc solid only for pressures lower than $P_{SS}(<P_{FS})$, that is, in a region where the fluid is the stable phase (however, at $T^*=4.25$, a pressure P_{SS} simply does not exist, i.e., the bcc solid is never preferred to the fcc solid). Values of P_{SS}, P_{FS}, and of $\Delta\mu\equiv\mu_{FCC}-\mu_{BCC}$ (as calculated at the fluid-solid transition pressure P_{FS}) are reported in Table II for the various temperatures. In the same table, the values of the freezing and the melting densities are also indicated. All the tabulated quantities are reported with three decimal digits, with no indication of the estimated statistical errors. The general question of the numerical reliability of our results is postponed to the next section, but we can anticipate that the results are fully trustworthy.

Figure 2 shows the chemical potential excess $\Delta\mu(P)$ of the fcc phase relatively to bcc, for $T^*=16$. This quantity is larger than zero (i.e., the stable solid is of bcc structure) only inside the fluid region of the phase diagram. Hence, the fluid directly transforms into the fcc solid, while the bcc phase is metastable. In the same picture, we also plot the difference in chemical potential between fcc and hcp phases, a quantity that is nearly constant and close to −0.004 at all pressures. This means that the hcp solid is never stable, albeit it is about to be so at all pressures.

Considering the small μ gaps between the various solids, one may wonder whether the above conclusions are influ-

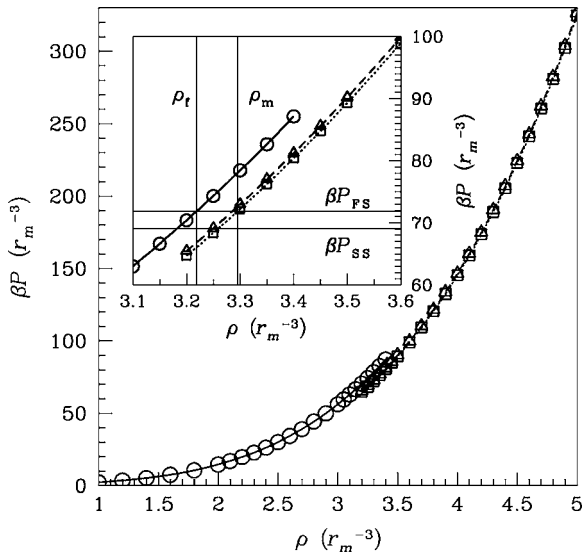

FIG. 3. Mechanical equation of state for $T^*=16$. The fluid branch (○ and continuous line) and the fcc branch (□ and dotted line) are plotted for $N=1372$ particles, while the bcc branch (△ and dashed line) is for a system of 1458 particles. In the inset, we zoom into the transition region: the freezing and melting densities (signaled by vertical lines) are located where the horizontal line at βP_{FS} crosses the fluid and fcc equations of state.

TABLE II. Phase-transition data for $T^*=4.25,8.15,12.77$, and 16. With the exception of $T^*=4.25$, simulation data refer to $N=1372$ (fluid and fcc) and $N=1458$ (bcc). For $T^*=4.25$, $N=864$ for fluid and fcc; no bcc phase was considered. From left to right, values of βP_{SS} (bcc-to-fcc "virtual" transition, falling inside the fluid region of the phase diagram), βP_{FS} (fluid-to-fcc transition), $\beta\mu_{FS}$ (common value of $\beta\mu$ for the coexisting fluid and fcc solid), $\beta\Delta\mu_{FS}$ (reduced chemical potential of fcc relative to bcc at $P=P_{FS}$), ρ_f (freezing density), and ρ_m (fcc melting density) are shown. These quantities were arbitrarily rounded off at the third decimal digit (the fourth digit only for $\beta\Delta\mu_{FS}$). However, the error accompanying them would usually be larger, originating from the limited precision of both the Monte Carlo data and the free-energy values in Table I.

T^*	$\beta P_{SS}(r_m^{-3})$	$\beta P_{FS}(r_m^{-3})$	$\beta\mu_{FS}$	$\beta\Delta\mu_{FS}$	$\rho_f(r_m^{-3})$	$\rho_m(r_m^{-3})$
4.25		28.897	18.774		1.980	2.055
8.15	40.979	46.883	25.565	−0.0124	2.496	2.571
12.77	57.445	62.238	29.519	−0.0060	2.946	3.022
16	69.130	71.877	31.552	−0.0029	3.219	3.295

enced by the finite size of the simulated samples. To this purpose, we have taken $T^*=16$ and plotted in Fig. 2 the same quantity $\Delta\mu(P)$ as before, but now calculated for a smaller fcc solid of 864 particles and for a bcc solid of 1024 particles. The new curve differs from the old one just for a small rigid shift toward low pressures, and crosses zero at $\beta P_{SS}=67.686r_m^{-3}$ (to be contrasted with the previous value of $69.130r_m^{-3}$). A bit smaller is the variation of βP_{FS} as N changes from 1372 to 864 (it moves from $71.877r_m^{-3}$ to $71.051r_m^{-3}$). We expect that similar results would be obtained at the other temperatures. Considering the large N values involved, it is very unlikely that our conclusions for the largest sizes can be reversed in the thermodynamic limit.

In Fig. 3, the various branches of the equation of state βP vs ρ are plotted for $T^*=16$. This curve shows a straight-line cut at $P=P_{FS}$, which allows one to identify the values of ρ_f and ρ_m for the given T. Correspondingly, the Helmholtz free energy shows, as a function of the specific volume $v=1/\rho$, a straight-line behavior in the interval between ρ_m^{-1} and ρ_f^{-1}. This line is the common tangent of the fluid and the fcc free-energy curves (its equation is $\beta f=\beta\mu_{FS}-\beta P_{FS}v$). Finally, a look at the RDFs in the coexistence region indicates that the typical values of the nearest-neighbor distance in all phases fall well within the repulsive shoulder of the pair potential, as expected for any highly compressed system.

An inspection of Table II shows that, as temperature grows, the difference $P_{FS}-P_{SS}$ gradually reduces until it would cross zero at $T^*\approx 19$, as suggested by a power-law extrapolation beyond $T^*=16$ of $P_{SS}(T)$ and $P_{FS}(T)$. Originally, it was just this evidence that led us to include in our calculations two other isotherms at $T^*=20$ and 25, in order to see whether a bcc-fcc phase transition eventually shows up at very high temperatures. Indeed, when T^* is as high as 20, we find that, on increasing pressure, the sequence of stable phases of the exp-6 model is fluid-bcc-fcc, with transitions at $\beta P_{FS}=83.517r_m^{-3}$ (fluid-to-bcc transition) and at $\beta P_{SS}=83.575r_m^{-3}$ (bcc-to-fcc transition). Actually, at this temperature the bcc window is so narrow that the fluid-bcc-fcc triple temperature should be very close to $T^*=20$. At $T^*=25$, the interval of stability of the bcc phase is much wider ($\approx$6 GPa). Table III reports thermodynamic data for $T^*=20$ and 25, whereas the difference in chemical potential between the various phases is shown in Fig. 4 for $T^*=25$ as a function of pressure. Hence, the bcc phase becomes eventually stable, but at much higher temperatures than estimated in Ref. 5.

In the end, the P-T phase diagram of the exp-6 model would appear as in Fig. 5, where temperature and pressure are reported in Xe units. In this picture, our fluid-solid coexistence data are contrasted with the coexistence loci of Belonoshko *et al.* and with the Simon-Glatzel equation of state for Xe, as deduced from that of Ne by the simple rescaling of pressure and temperature values proposed by Vos *et al.*[29] Compared to the findings of Ref. 5, freezing of the exp-6 system occurs for slightly lower pressures in our simulation; more important, our fluid-fcc-bcc triple point lies very far from the location indicated by Belonoshko *et al.*

To better understand the nature of the differences between our results and those of Belonoshko *et al.*, we have plotted in Fig. 6 the exp-6 phase diagram on the T-V plane. It can be appreciated from this picture that small differences in the volumes of the coexisting fluid and fcc solid are found at all temperatures. On the contrary, isobaric paths are pretty much the same (see Fig. 11 of Ref. 5 for a comparison), indicating that where we deviate from Belonoshko *et al.* is essentially

TABLE III. Phase-transition data for $T^*=20$ and 25. From left to right, values of βP_{FS} (fluid-to-bcc transition), βP_{SS} (bcc-to-fcc transition), ρ_f (freezing density), ρ_m (bcc melting density), ρ_{bcc} (bcc density at the bcc-fcc transition), and ρ_{fcc} (fcc density at the bcc-fcc transition) are shown.

T^*	$\beta P_{FS}(r_m^{-3})$	$\beta P_{SS}(r_m^{-3})$	$\rho_f(r_m^{-3})$	$\rho_m(r_m^{-3})$	$\rho_{bcc}(r_m^{-3})$	$\rho_{fcc}(r_m^{-3})$
20	83.517	83.575	3.533	3.601	3.602	3.611
25	96.901	103.84	3.888	3.958	4.039	4.048

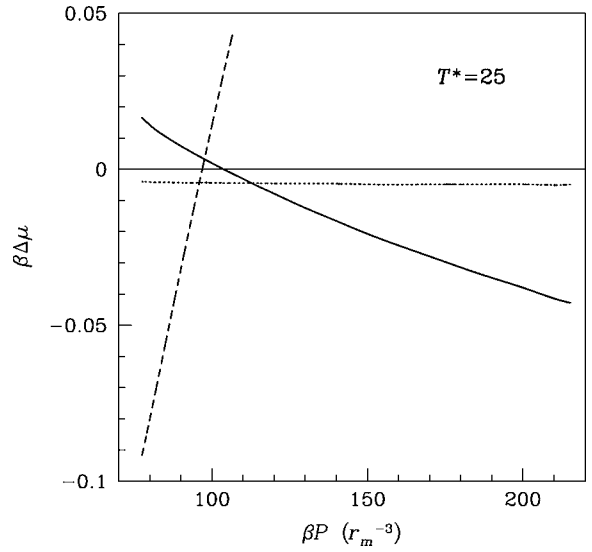

FIG. 4. Reduced chemical potential of the fcc ($N=1372$) phase relative to bcc ($N=1458$, continuous line) and hcp ($N=1440$, dotted line), and of the fluid phase ($N=1372$) relative to bcc ($N=1458$, dashed line), for $T^*=25$. Upon increasing pressure, we observe a fluid-bcc-fcc sequence of phases.

in the definition of the phase-coexistence condition, not in the calculation of basic statistical averages.

Where we radically contrast with Belonoshko *et al.* is really in the position of the bcc-fcc transition line, with ours running much higher in temperature and pressure. To assess how distant is our prediction from these authors, we note that, for, e.g., $T^*=16$, they report a reduced pressure of about 70 GPa ($P^*/T^* \simeq 120$) at the bcc-fcc transition while, at the same pressure, our $\beta\Delta\mu$ is about -0.040 (see Fig. 2), i.e.,

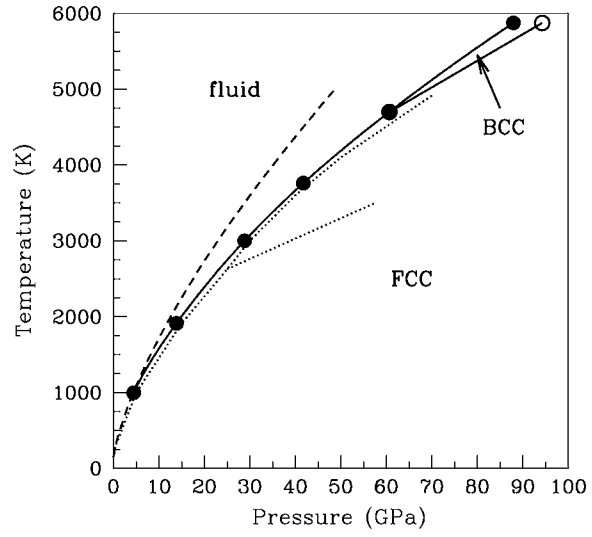

FIG. 5. HT-HP phase diagram of the exp-6 model (temperature and pressure are rescaled using Ross parameters for Xe). Besides our data (full and open dots), we plot the coexistence loci for the exp-6 model as calculated by Belonoshko *et al.* (dotted lines), and the Xe freezing line as derived—after suitable rescaling of temperature and pressure values—from the Simon-Glatzel fit of Ne data by Vos *et al.* (dashed line).

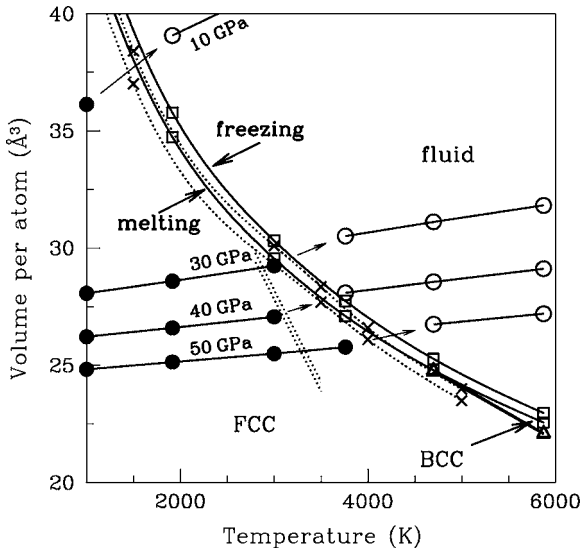

FIG. 6. Volume-temperature phase diagram of Xe as drawn from our numerical simulation of the exp-6 model. Present data for the melting and the freezing volumes (□ and continuous lines) and for the bcc-fcc coexistence volumes (△ and straight lines) are compared with the estimates by Belonoshko *et al.* (× and dotted lines, as obtained from Fig. 11 of Ref. 5). Following Fig. 11 of the cited reference, we have also plotted as circles some isobars (open circles, fluid; full dots, fcc solid).

appreciably larger, in absolute terms, than the size of statistical errors.

IV. DISCUSSION

Having devoted the last section to a plain presentation of our results, we now reconsider more critically their implications, especially in relation to the numerical precision of the simulation data.

The crucial quantity to look at is, obviously, the chemical potential. One source of error in its calculation follows from the finite size of the simulated system, a problem further complicated by the impossibility of comparing fcc and bcc solids with equal numbers of particles. In point of principle, this would force us to some sort of extrapolation to $N=\infty$ which, however, is computationally demanding. Instead, we have decided to simulate fluid, fcc, bcc, and hcp samples of similar size, which are also sufficiently large that no significant finite-size error would be made in tracing the coexistence lines. Indeed, we have already demonstrated in the previous section—see the comment on Fig. 2—that this kind of error is not very important.

Further errors in estimating the relative stability of two distinct solid phases are imputable to the limited precision with which we compute the excess free energy of the reference solid states in Table I as well as the pressure values along an isothermal path. Looking at Table I, the overall error on the free-energy difference between bcc and fcc phases in units of k_BT is about three units on the third decimal place, and comparable is the statistical error accompanying the values of $\beta P/\rho$ for each phase. The error associ-

ated with the $\beta\mu$ gap between the fluid and a solid phase is again about $(4–5)\times 10^{-3}$, but the rate at which this quantity varies as a function of pressure is much larger (this implies that the location of the fluid-solid transition is much better defined numerically than is the solid-solid transition point). Summing up, we expect that the typical statistical error affecting the bcc-fcc $\beta\Delta\mu$ is about 10^{-2}. If this is true, it is evident from the tabulated values of $\beta\Delta\mu$ that we cannot definitely rule out the possibility that the bcc solid becomes stable at temperatures lower than $T^*=20$, and even as small as 11. Only if we turn to much longer Monte Carlo runs than hereby considered can we hope to reduce drastically the width of the error bars. Anyway, even in the worst case, we can safely infer from our data that the bcc phase may only be stable in a narrow slice of a few gigapascals adjacent to the fluid-bcc coexistence locus, a pressure interval much narrower than predicted by Belonoshko *et al.*

The caution expressed above is probably overstated: it is a fact that all the curves plotted in Figs. 2 and 4 are very smooth, which suggests that the statistical noise underlying the profile of $\beta\Delta\mu$ is considerably smaller than the *maximum* estimated above. In this case, the conclusions drawn in the previous section just on the basis of the *average* behavior of $\Delta\mu$ are substantially correct, and the bcc phase will really be metastable below $T^*\approx 20$. If we believe this, a stable bcc phase would first appear in Xe at so high a temperature ($\approx$4500 K) that one can even wonder whether the bcc-fcc transition in Xe is preempted by quantum effects.

As a matter of fact, our simulation results do not match the experimental data of Boehler *et al.* at the highest temperatures. Even assuming that the exp-6 system is a very good representation of Xe in the HT-HP regime, the problem could be in fact with the experiment, which might be far from realizing hydrostatic conditions. In fact, it is generally believed that, in a laser-heated DAC experiment, the stress state within the diamond cell may not be hydrostatic; moreover, the sample can even exhibit considerable shear stresses.[30] In consideration of the small difference in chemical potential between bcc, fcc, and hcp phases, it could then be that what is experimentally recognized as solid is in fact a mixture of bcc and fcc-hcp crystallites.

V. CONCLUSIONS

In this paper, we have reported on the results of an extensive *NVT* Monte Carlo simulation of the exp-6 model, an effective-interaction model that is thought to provide a realistic description of the thermal properties of rare gases under extreme, high-temperature–high-pressure conditions. We have plotted the "exact" phase diagram of this system upon combining the method of thermodynamic integration with fully fledged free-energy calculations both in the fluid (by the Widom method) and in the solid phase (by the Frenkel-Ladd method).

The aim of this effort was to point out some aspects concerning the uncertain status of the solid phase of xenon at high densities. In a previous molecular-dynamics study of the exp-6 system, with parameters being appropriate to Xe, the two-phase method was employed for simulating the thermodynamic coexistence between fluid and solid.[5,10] This study gave evidence of a stable bcc phase in a narrow range of pressures above 25 GPa, when temperature exceeds 2700 K, i.e., near to where a laser-heated, diamond-anvil-cell experiment finds a cusp on the freezing line of Xe. In fact, our free-energy calculations partially contradict such findings, showing that Xe freezes directly into a fcc solid, the bcc phase becoming stable only at much higher temperatures (above 4500 K), provided that the exp-6 modelization is still valid for Xe in these extreme conditions; moreover, the hcp solid is practically as stable as the fcc one.

A clue to understanding this disagreement is the very small difference in Gibbs free energy, for $T>2500$ K, between the bcc and fcc solids of equal pressure and similar size. The little advantage of fcc over bcc at freezing could be the reason for the apparent stability of the bcc phase in the former numerical study of the exp-6 model. In our simulation study, we find that, at sufficiently high temperature, there is a narrow range of pressures where the bcc solid is more stable than the fcc, but less stable than the fluid. Only beginning from $T^*=20$, the bcc phase gains true thermodynamic stability in an interval of pressures. Obviously, this careful monitoring of the relative stability of the various phases as a function of both temperature and pressure would simply be impossible without the knowledge of their respective chemical potentials, and this is the ultimate reason for preferring exact free-energy calculations to other methods.

As far as the experiment is concerned, it is likely that the cusplike feature on the Xe freezing line is just an experimental artifact, which could be due to the increasing difficulty, as the freezing density progressively grows, in establishing hydrostatic conditions, a problem also worsened by the existence of two different solid phases that so closely compete with each other for stability.

*Email address: saija@me.cnr.it
†Corresponding author. Email address: Santi.Prestipino@unime.it

[1] R. J. Hemley and N. W. Ashcroft, Phys. Today **51** (8), 26 (1998).
[2] S. Scandolo and R. Jeanloz, Am. Sci. **91**, 516 (2003).
[3] J. A. Shouten, J. Phys.: Condens. Matter **7**, 469 (1995).
[4] A related puzzle is the unexpectedly low abundance of Xe in the Earth's atmosphere. The existence of dense solid and fluid inclusions of rare gases in the Earth's interior would provide a resolution for this paradox—see, e.g., A. P. Jephcoat, Nature (London) **393**, 355 (1998).
[5] A. B. Belonoshko, O. Le Bacq, R. Ahuja, and B. Johansson, J. Chem. Phys. **117**, 7233 (2002).
[6] P. Loubeyre, Phys. Rev. B **37**, 5432 (1988).
[7] R. A. Buckingham, Proc. R. Soc. London, Ser. A **168**, 264

(1938).
[8] M. Ross and A. K. McMahan, Phys. Rev. B **21**, 1658 (1980).
[9] R. Boehler, M. Ross, P. Soderlind, and D. B. Boercker, Phys. Rev. Lett. **86**, 5731 (2001).
[10] A. B. Belonoshko, R. Ahuja, and B. Johansson, Phys. Rev. Lett. **87**, 165505 (2001).
[11] See V. V. Kechin, Phys. Rev. Lett. **89**, 119601 (2002),and the subsequent reply by A. B. Belonoshko, R. Ahuza, and B. Johansson, *ibid.* **89**, 119602 (2002).
[12] J. R. Morris, C. Z. Wang, K. M. Ho, and C. T. Chan, Phys. Rev. B **49**, 3109 (1994).
[13] J. R. Morris and X. Song, J. Chem. Phys. **116**, 9352 (2002).
[14] A. B. Belonoshko, Geochim. Cosmochim. Acta **58**, 4039 (1994).
[15] R. Agrawal and D. A. Kofke, Phys. Rev. Lett. **74**, 122 (1995).
[16] D. Frenkel and A. J. C. Ladd, J. Chem. Phys. **81**, 3188 (1984).
[17] D. Frenkel, Phys. Rev. Lett. **56**, 858 (1986).
[18] F. W. Tavares and S. I. Sandler, Mol. Phys. **87**, 1471 (1996).
[19] J. R. Errington and A. Z. Panagiotopoulos, J. Chem. Phys. **109**, 1093 (1998).
[20] H. L. Vortler, I. Nezbeda, and M. Lizal, Mol. Phys. **92**, 813 (1997).
[21] M. Lizal, I. Nezbeda, and H. L. Vortler, Fluid Phase Equilib. **154**, 49 (1999).
[22] A. K. McMahan, Phys. Rev. B **33**, 5344 (1986).
[23] A. P. Jephcoat, H.-k. Mao, L. W. Finger, D. E. Cox, R. J. Hemley, and C.-s. Zha, Phys. Rev. Lett. **59**, 2670 (1987).
[24] D. Errandonea, B. Schwager, R. Boehler, and M. Ross, Phys. Rev. B **65**, 214110 (2002).
[25] M. I. Eremets, E. A. Gregoryanz, V. V. Struzhkin, H. K. Mao, R. J. Hemley, N. Mulders, and N. M. Zimmerman, Phys. Rev. Lett. **85**, 2797 (2000).
[26] J. M. Polson, E. Trizac, S. Pronk, and D. Frenkel, J. Chem. Phys. **112**, 5339 (2000).
[27] D. Frenkel and B. Smit, *Understanding Molecular Simulation* (Academic Press, San Diego, 1996).
[28] This follows from a straightforward application of the rules of functional calculus: if we call the functional $\int_a^b dx\, f(x) I[f]$, the first variation of I is given by $\delta I[f] = \int_a^b dx\, \delta f(x)$.
[29] W. L. Vos, J. A. Schouten, D. A. Young, and M. Ross, J. Chem. Phys. **94**, 3835 (1991).
[30] A. Kavner and T. S. Duffy, J. Appl. Phys. **89**, 1907 (2001).